Intermolecular potential energy surfaces and bound states in F–HF

Markus Meuwly and Jeremy M. Hutson

Citation: The Journal of Chemical Physics **112**, 592 (2000); doi: 10.1063/1.480552
View online: http://dx.doi.org/10.1063/1.480552
View Table of Contents: http://scitation.aip.org/content/aip/journal/jcp/112/2?ver=pdfcov
Published by the AIP Publishing

Intermolecular potential energy surfaces and bound states in F–HF

Markus Meuwly and Jeremy M. Hutson
Department of Chemistry, University of Durham, South Road, Durham DH1 3LE, England

(Received 9 September 1999; accepted 12 October 1999)

Semiempirical potential energy surfaces for F–HF are constructed, based on recent Ne–HF, Ne–F, and Ne–Ne potentials. The electrostatic forces due to the quadrupole of the F atom are included. The potentials are presented in diabatic and adiabatic representations, with and without spin–orbit coupling. Fully coupled bound-state calculations are carried out, and the resulting energy levels and wave functions are analyzed. The well depth is $317\,\mathrm{cm}^{-1}$, and the ground state is bound by $174\,\mathrm{cm}^{-1}$. The complex is a promising candidate for spectroscopic observation, which would provide detailed information on the potential energy surfaces in the entrance and exit valleys of the F+HF reaction. © *2000 American Institute of Physics.* [S0021-9606(00)00502-X]

I. INTRODUCTION

Over the last 20 years, studies of van der Waals complexes have provided a great deal of information on both pairwise and nonadditive intermolecular forces. The early work in this area concentrated on interactions between closed-shell species, and the concerted application of experiment and theory resulted in accurate and reliable intermolecular potential energy surfaces for a range of prototype systems.[1–6] There is now growing interest in open-shell complexes,[7–10] where much less is known about the interactions involved. There is an excellent prospect that similar advances can be made in the open-shell case.

A particularly interesting class of open-shell complexes are those in which an open-shell atom interacts with a closed-shell diatom. Atoms in *P* states can have substantial quadrupole moments, so such species can be relatively strongly bound. Some of them are ''prereactive'' complexes, which offer the opportunity of investigating the influence of long-range forces on chemical reactions. In particular, symmetric heavy–light/heavy X–HX complexes provide an attractive platform for detailed studies of hydrogen exchange reactions. Most of the previous work on such reactions has focussed on the transition-state region, which is at relatively high energy.

Even with recent advances in *ab initio* techniques, the construction of reliable potential energy surfaces for such an open-shell system is a formidable task. At least three potential energy surfaces are needed to describe the interaction of an atom in a *P* state with a closed-shell molecule. For nonlinear geometries, two of the potential energy surfaces are of the same symmetry. The complications include the calculation of nonadiabatic coupling matrix elements and relativistic effects due to spin–orbit interaction. Under these circumstances, semiempirical models are of considerable value.

Dubernet and Hutson[10] developed a model for the potential energy surfaces of X–HX systems, valid at long range, and applied it to Cl–HCl. Their model gave a van der Waals well $383\,\mathrm{cm}^{-1}$ deep, principally due to electrostatic interactions; this was considerably deeper than previous potentials designed for reactive scattering calculations. Dubernet and Hutson carried out bound-state calculations for Cl–HCl; they obtained a ground-state binding energy of $219\,\mathrm{cm}^{-1}$, and gave predictions for various spectroscopic transitions that are potentially observable. Subsequently, Maierle *et al.*[11] combined the long-range surfaces of Ref. 10 with surfaces for the reactive region based on MCSCF calculations, and used the resulting potentials for reactive scattering calculations; they showed that the attractive well has important effects on the reactive scattering, especially on the location of reactive scattering resonances. Recently, Dobbyn *et al.*[12] have extended this work to use higher-level *ab initio* calculations.

The X–HX systems are also topical because of recent experiments by Wittig and co-workers,[13] in which HCl in HCl dimer is photodissociated and the kinetic energy of the resultant H atoms is measured. Wittig and co-workers have interpreted the structure they observe in terms of photodissociation to form a Cl–HCl fragment, and have used the potential energy surfaces of Dubernet and Hutson[10] in their analysis. Since other HX dimers are accessible to similar experiments, it is timely to extend the work on Cl–HCl to analogous complexes containing other halogens.

The purpose of the present work is to describe model potential energy surfaces for F–HF, and to investigate the bound states that they support. The F–HF reaction is another prototype hydrogen exchange reaction, and the F–HF van der Waals complex is a good candidate for spectroscopic observation. Measurements of its bound states would lead to improved understanding of the reaction, especially for processes that occur in the entrance and exit valleys. In addition, F–HF is likely to be an important product in the UV photodissociation of the HF dimer.

The reduced number of electrons in F–HF compared to Cl–HCl makes the former an attractive target for high-level *ab initio* calculations, which would be valuable to assess the accuracy of the potential models used in the present work. Preuss *et al.*[14] and more recently Bittererová and Biskupič[15] have investigated the stationary points on the ground and excited potential surfaces of FHF, and their results will be compared with ours below. Bittererová and Biskupič[15] also gave a useful summary of the early *ab initio* work on the system, which focused on the reaction pathway.

Charged FHF species are also of interest. Matrix isolation and IR diode laser studies have been performed on FHF^- (Ref. 16) and FDF^- (Ref. 17) and the reactivity of HF_2^+ has recently been investigated.[18]

The present article is structured as follows. Section II describes the construction of a semiempirical interaction potential, based on recent Ne–HF and Ne–F potentials. Section III reports bound-state calculations of various levels of sophistication. Predictions for experimentally observable states are made. The energy level pattern is described, and interpreted with the aid of vibrational wave functions. The predissociating states correlating with F ($^2P_{1/2}$) are also investigated. Finally, Sec. IV presents our conclusions.

II. THEORETICAL APPROACH

The present work uses a standard Jacobi coordinate system, in which r is the F–H distance, R is the distance from the HF center-of-mass to F, and θ is the angle between r and R, measured at the HF center-of-mass (with $\theta=0$ corresponding to the linear F–H–F geometry). Vibrations of the HF monomer are not considered explicitly in the present work, and the potentials obtained here should be considered to be averages over the vibrational motion of HF.

Open-shell species are more complicated than closed-shell species because they contain additional sources of angular momentum that can couple together in various ways. An unpaired electron contributes both spin and electronic orbital angular momentum, and there are also angular momenta arising from the rotation of the diatomic molecule and the rotation of the atom and the diatom about one another. As is customary for van der Waals complexes, lower-case letters are used here for quantities that refer to the monomers and upper-case letters for those that refer to the complex.[8] Thus the total orbital and spin quantum numbers of the F atom are denoted l and s, with resultant j_a and projection ω onto the intermolecular axis. The rotational angular momentum of the HF monomer is denoted j, and its rotational constant is b. The total angular momentum of the complex is denoted J and the corresponding rotational constant is B.

The interaction between an atom in a P state and a diatomic molecule can be described in terms of three diabatic or adiabatic (Born–Oppenheimer) surfaces.[19] The dynamics involve all three surfaces and the couplings between them. Because of this, the Born–Oppenheimer surfaces themselves are not enough to understand the dynamics: additional information on the electronic wave functions is required to calculate the coupling matrix elements.

For dynamical calculations, it is more convenient to use a diabatic than an adiabatic representation of the potentials. To a first approximation, the intermolecular interaction is too weak to mix in excited atomic orbitals of the halogen atom, and the atomic orbital angular momentum l is nearly conserved. In the absence of spin–orbit coupling, the three diabatic surfaces are those for interaction of HX with an X atom with its unpaired electron in a pure p_x, p_y, or p_z orbital (where the z-axis is along the intermolecular vector R and the three atoms lie in the xz-plane). An alternative way to view this is to introduce angles θ_a and ϕ_a that are conjugate to l and m_l: in a simple picture, θ_a and ϕ_a may be thought of as the angular coordinates of the unpaired electron. The resulting potential surface depends on the intermolecular distance R and three angles, θ, θ_a, and ϕ_a.

A. Model potential for F–HF

There are not yet any reliable *ab initio* calculations of the potential surfaces needed for bound-state calculations on F–HF. Indeed, the theoretical methods and expertise needed for such calculations are only just being developed. We have therefore followed the same procedure as in the earlier work on Cl–HCl to construct an intermolecular potential for F–HF, incorporating the electrostatic terms arising from the open-shell character of the F atom.[10] The model is based on analogies with related systems such as Ne–Ne, Ne–HF, and Ne–F.

For spectroscopic calculations, it is important to model the anisotropy of the potential surface as accurately as possible. In a system such as F–HF, both the atom and the molecule are anisotropic. The potential energy surface may be expanded

$$V(R,\theta,\theta_a,\phi_a)=\sum_{\lambda_r\lambda_a\lambda_{12}} V_{\lambda_r\lambda_a\lambda_{12}}(R)\mathcal{I}_{\lambda_r\lambda_a\lambda_{12}}. \tag{1}$$

The functions $\mathcal{I}_{\lambda_r\lambda_a\lambda_{12}}$ are explained in detail in Ref. 10. They describe linear combinations of (space-fixed) spherical harmonics, weighted by the appropriate Clebsch–Gordan coefficients.

A first source of anisotropy involves terms similar to those that arise in Ne–HF, which are essentially due to the shape of the HF monomer. The Ne–HF interaction is conveniently expanded as

$$V_{\mathrm{Ne-HF}}(R,\theta)=\sum_{\lambda_r} V_{\lambda_r}(R)P_{\lambda_r}(\cos\theta). \tag{2}$$

The interaction between Ne and HF has recently been determined by a ''morphing'' procedure,[20] using data from high-resolution spectroscopy to modify good quality *ab initio* potential energy surfaces. Since the F atom is similar in size to the Ne atom, the Ne–HF terms $V_{\lambda_r}(R)$ were carried over unchanged to F–HF. In the total potential (see below), these terms contribute anisotropic terms $V^{\lambda_r 0\lambda_r}(R)$ to the F–HF potential.

A second source of anisotropy involves terms similar to those that exist for Ne–F, and reflect the shape of the F atom. The Ne–F potential can be expanded

$$V_{\mathrm{Ne-F}}(R,\theta_a)=\sum_{\lambda_a=0,2} V_{\lambda_a}(R)P_{\lambda_a}(\cos\theta_a). \tag{3}$$

These contributions are also used unchanged and give rise to anisotropic terms $V^{0\lambda_a\lambda_a}(R)$ with $\lambda_a=0$ or 2.

In addition, electrostatic terms V_{Q} arise from the interaction of the atomic quadrupole on F with the multipoles on HF. These can be approximated

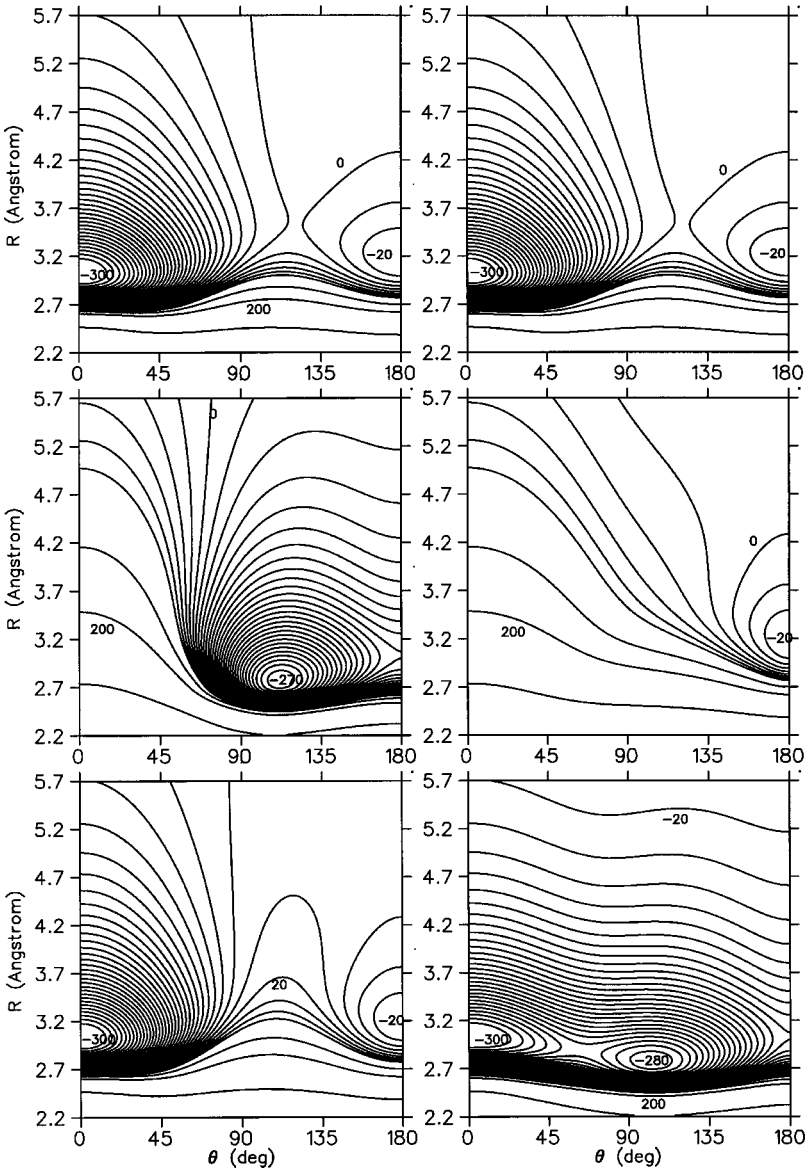

FIG. 1. Contour plots of the interaction potentials excluding spin. Diabatic surfaces (p_y, p_z, p_x from top to bottom) are shown on the left and adiabatic surfaces ($1A''$, $2A'$, $1A'$ from top to bottom) on the right. Contours are drawn every $10\,\mathrm{cm}^{-1}$ up to $+50\,\mathrm{cm}^{-1}$ and at 100, 200, and $1000\,\mathrm{cm}^{-1}$.

$$V_{\mathrm{Q}}(R,\theta,\theta_a,\phi_a)=\frac{\sqrt{15}e\langle r_a^2\rangle\mu_m\mathcal{I}_{123}}{R^4}+\frac{\sqrt{70}e\langle r_a^2\rangle\Theta_m\mathcal{I}_{224}}{R^5}, \tag{4}$$

where μ_m and Θ_m are the permanent dipole and quadrupole of HF and $\langle r_a^2\rangle$ is the mean-square radius of the incomplete atomic shell. This is related to the permanent atomic quadrupole moment Θ_a by $\Theta_a=\frac{2}{5}e\langle r_a^2\rangle$. The value $\langle r_a^2\rangle=1.5438\,a_0$ is used in the present work.[21]

The complete F–HF potential is thus approximated by

$$V_{\mathrm{F-HF}}(R,\theta,\theta_a,\phi_a)=V_{\mathrm{Ne-HF}}(R,\theta)+V_{\mathrm{Ne-F}}(R,\theta_a)-V_{\mathrm{Ne-Ne}}(R)+V_{\mathrm{Q}}(R,\theta,\theta_a,\phi_a). \tag{5}$$

In the present work, $V_{\mathrm{Ne-F}}(R,\theta_a)$ is the Ne–F potential of Aquilanti *et al.*,[22] and $V_{\mathrm{Ne-Ne}}(R)$ is the Ne–Ne potential of Aziz and Slaman.[23]

B. Spin-free representation

The different possible ways of representing the interaction potential are explained in detail in Ref. 10. The following discussion is thus restricted to features specific to the F–HF interaction.

Figure 1 shows contour plots of the diabatic and adiabatic surfaces in the spin-free representation. For the diabatic surfaces, the unpaired electron on the F atom is forced to remain in an individual p orbital with definite orientation. The p_x and p_y diabatic surfaces each show a deep minimum at the linear F–HF geometry. Between this minimum and the secondary minimum at the F–FH geometry is a saddle point. The secondary minima are much shallower for F–HF than for Cl–HCl. The p_z diabatic surface is quite different, with a single minimum at a T-shaped geometry.

The shapes of the spin-free diabatic surfaces can be rationalized in terms of the electrostatic interaction between F and HF. An F atom with a partially filled p orbital has a quadrupole moment oriented along the axis of the orbital.

For a partially filled p_x or p_y orbital, the ring of negative charge around the equator of the F atom faces the HF molecule. Since the hydrogen atom carries a partial positive charge, the linear F–HF configuration is favored. For a partially filled p_z orbital, the positive end of the quadrupole points towards the HF. In this case, the partial positive charge on the hydrogen atom makes the linear F–HF configuration repulsive. If HF were a purely dipolar molecule, the equilibrium geometry for the p_z diabat would be F–FH. However, HF also has a substantial quadrupole, and the quadrupole–quadrupole interaction favors a T-shaped geometry.

The p_x and the p_y surfaces are degenerate for $\theta=0$ and 180°, so the two diabatic surfaces have identical well depths. However, the two surfaces diverge as the geometry departs from linear. In each case there is a saddle point at a T-shaped geometry.

The potential surfaces can be expressed in an adiabatic form by diagonalizing a matrix representation of the potential in the basis set of atomic functions for $l=1$. The diagonal elements of this matrix are the diabats and mixing between p_x and p_z is introduced through off-diagonal elements as described in Ref. 10. There are two surfaces of A' symmetry and one of A'' symmetry. Because the A'' adiabat is not coupled to the other two, it is identical to the p_y diabat. The lower of the two A' surfaces has an absolute minimum at the linear configuration arising from the p_x diabat and a secondary minimum near the T-shaped geometry arising from the p_z diabat. These two minima are separated by a saddle point about 60 cm^{-1} above the global minimum.

The spin-free adiabats are the appropriate surfaces for comparison with *ab initio* surfaces that neglect spin–orbit coupling. The most recent such calculations are by Bittererová and Biskupič,[15] who carried out multireference configuration interaction (MRCI-SD) calculations to characterize the stationary points using basis sets of up to triple-zeta quality. They carried out sets of calculations that can be compared with our surfaces. They first started from the F–F–H geometry, from which they located a nonlinear minimum with well depth 0.880 kcal mol^{-1} (308 cm^{-1}) at $r=1.750\,a_0$, $R_{\mathrm{FF}}=4.936\,a_0$, and $\theta_{\mathrm{FFH}}=113°$. This H–F bond length is only $0.01\,a_0$ longer than for the HF monomer, which justifies our fundamental assumption that F–HF can be treated as though it contains a weakly perturbed HF monomer. Their geometry corresponds to $R=4.971\,a_0$ and $\theta=114°$ in our coordinate system, which compares with our secondary minimum (on the lower A' surface) at $R=5.216\,a_0$ and $\theta=103°$; our minimum has depth 288 cm^{-1}.

The FFH bond length/bond angle coordinate system does not lend itself to studying linear F–HF geometries. Accordingly, Bittererová and Biskupič carried out separate calculations at these geometries, and found a linear F–HF minimum with $r=1.72\,a_0$, $R_{\mathrm{FH}}=4.31\,a_0$, and well depth 1.42 kcal mol^{-1} (497 cm^{-1}). This distance corresponds to $R=5.972\,a_0$ and may be compared with our absolute minimum at $R=5.716\,a_0$ and 317 cm^{-1}. It thus appears that our surfaces agree in general shape with the best existing *ab initio* calculations, but have rather smaller well depths. However it should be noted that the energies in Ref. 15 are not corrected for basis set superposition error. Further evidence is needed to decide which is better.

C. Representation including spin

The spin–orbit coupling in the F atom is comparable in magnitude to the separations between the spin-free potential surfaces. Either it can be regarded as coupling the spin-free states, or it can be included in the description of the potential surfaces. To do the latter, the spin–orbit coupling in the complex is assumed to be unchanged from that in the isolated F atom, and to be of the form $\xi\hat{\mathbf{l}}\cdot\hat{\mathbf{s}}$. The matrix representation is constructed in a basis including atomic orbital functions for $l=1$ and spin functions for $s=1/2$, with resultant $j_a=1/2$ or 3/2 and projection ω onto the intermolecular axis. The resulting 6×6 matrix has three pairs of equal diagonal elements and three doubly degenerate pairs of eigenvalues; either the diagonal elements (diabats) or the eigenvalues (adiabats) can be plotted. Contour plots of the resulting surfaces are shown in Fig. 2.

The lowest two diabatic surfaces correspond to $j_a=3/2$ with $|\omega|=3/2$ and 1/2. The third corresponds to $j_a=1/2$, $|\omega|=1/2$, and is thus shifted upwards at long range by the atomic spin–orbit splitting ($\frac{3}{2}\xi$, where $\xi=-269.3\,\mathrm{cm}^{-1}$). The $j_a=3/2$, $|\omega|=3/2$ surface is fairly similar to the spin-free p_x diabat. However, the $j_a=3/2$, $|\omega|=1/2$ potential is quite different from the p_z diabat. There is also a marked difference between the $j_a=1/2$ diabat and the spin-free p_y surface. This arises because an atomic state with $j_a<1$ cannot have an overall quadrupole moment. This follows from the properties of the Clebsch–Gordan coefficients relating j_a and the quadrupole moment operator. The attractive electrostatic components thus make no contribution to the $j_a=1/2$ diabat; its anisotropy arises solely from the anisotropy of the Ne–HF potential.

It is also possible to extract adiabatic potential energy surfaces including spin. The resulting surfaces correlate at long range with either F ($^2P_{3/2}$) or ($^2P_{1/2}$). The double-minimum structure of the spin-free A' adiabat is carried over, whereas the analogue of the second A' adiabat is significantly changed. It has a double-minimum structure, with well depths of 104 cm^{-1} at the F–HF structure and 29 cm^{-1} at the HF–F structure, and a saddle point in between. The $j_a=1/2$ adiabat is even shallower than the $j=1/2$ diabat, again with its asymptote shifted upwards by the atomic spin–orbit splitting.

III. BOUND-STATE CALCULATIONS

We have used the BOUND program[24] to carry out helicity decoupled and close-coupling calculations of the bound vibrational–rotation states supported by the model potential for F–HF. The methods used have been described in detail in Ref. 10. The total wave function is expanded using rigid rotor functions for HF and coupled angular momentum basis functions for the complex as a whole. The resulting coupled equations are solved numerically using a log-derivative propagator.[25] The methods used to solve the coupled equations are described in detail in Ref. 26.

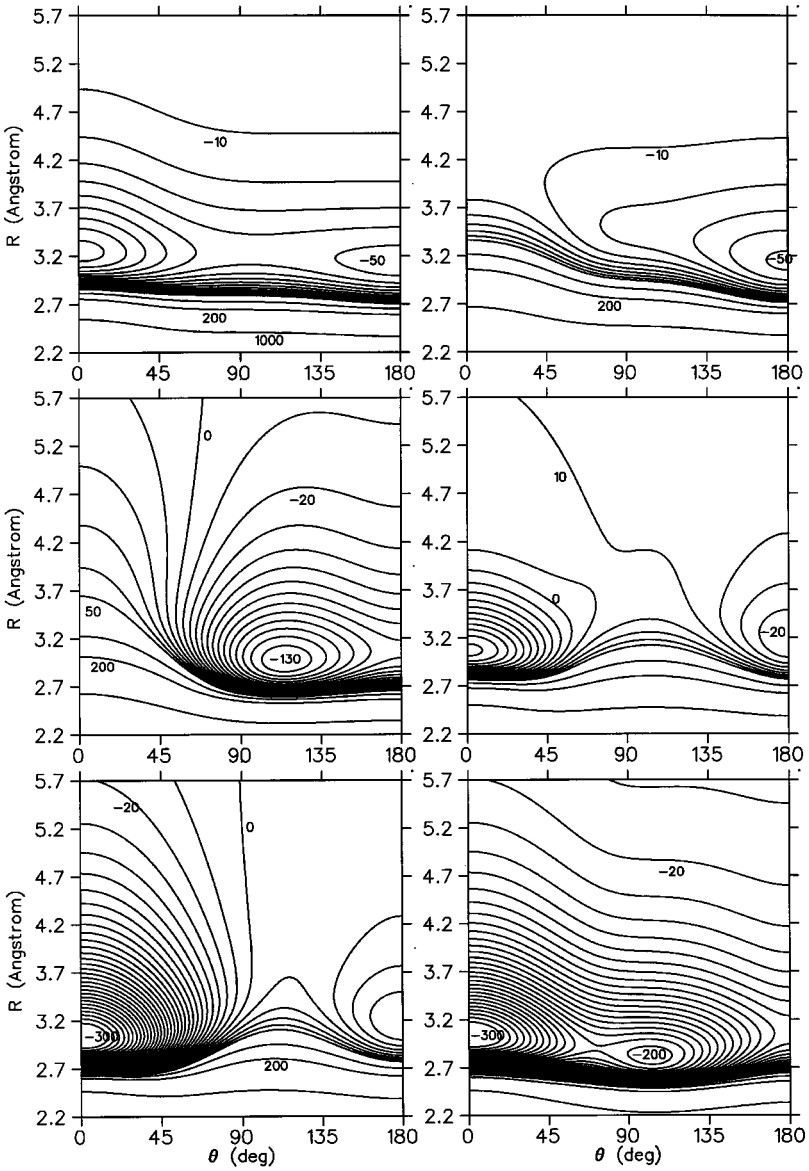

FIG. 2. Contour plots of the interaction potential including spin. Diabatic surfaces $[(j_a,|\omega|)=(1/2,1/2)$, $(3/2,1/2)$, $(3/2,3/2)$ from top to bottom] are shown on the left and adiabatic surfaces on the right. Contours are drawn every 10 cm^{-1} up to $+50$ cm^{-1} and at 100, 200, and 1000 cm^{-1}.

The HF molecule is treated as a rigid rotor with a rotational constant $b=19.787\,478\,\mathrm{cm}^{-1}$ corresponding to the $v=1$ state in HF. This choice is made because the Ne–HF potential is constructed for $v_{\mathrm{HF}}=1$.[20] The basis set includes all monomer functions up to $j=10$.

The F–HF reduced mass is taken to be 9.744 6461 m_u (where $m_u=m_a(^{12}\mathrm{C})/12$). The coupled equations are propagated from $R_{\min}=2$ Å to $R_{\max}=8$ Å extrapolating to zero step size from log-derivative interval sizes of 0.04 and 0.08 Å using Richardson h^4 extrapolation. Increasing the propagation range or decreasing the step size changes the eigenvalues by less than $10^{-4}\,\mathrm{cm}^{-1}$.

A. Helicity decoupling calculations

In the helicity decoupling approximation, the basis functions are labeled by P, the projection of the total angular momentum J onto the intermolecular axis, and terms off-diagonal in P are neglected. Such calculations give no information about parity splittings, and the rotational constants derived from them are approximate. Nevertheless, they provide a useful starting point for investigating the level patterns.

Helicity decoupling calculations were carried out for values of $|P|$ ranging from 1/2 to 5/2. The resulting energy levels are collected in Table I. No bound states with $|P|>5/2$ were found.

Before discussing the coupled channel calculations, it is useful to consider the structure of bending levels, uncomplicated by the intermolecular stretch. The left-hand side of Fig. 3 shows the pattern of bending levels, obtained by diagonalizing the helicity decoupled matrix at a fixed intermolecular distance, $R=3.0$ Å. It may be seen that, as for Cl–HCl, the lowest level has $|P|=3/2$. It can essentially be regarded as a bending state of a linear molecule with bending quantum number $v_b=0$, vibrational angular momentum $k=0$, and $|\omega|=3/2$. For F–HF, this state is bound by $174\,\mathrm{cm}^{-1}$, which is slightly less than in Cl–HCl.

The excited vibronic states are more difficult to interpret.

TABLE I. Energy levels and spectroscopic parameters from helicity decoupled calculations for F–HF. All quantities are given in cm^{-1}, with energy levels relative to the energy of $F(^2P_{3/2})+HF(j=0)$.

n	P	$J=1/2$	$J=3/2$	$J=5/2$	$J=7/2$
0	1/2	−136.850 47	−136.257 20	−135.268 81	−133.885 86
0	1/2	−99.592 66	−98.989 96	−97.985 83	−96.580 83
0,1	1/2	−87.808 97	−87.250 74	−86.320 94	−85.020 45
0,1	1/2	−78.353 28	−77.814 64	−76.917 17	−75.661 25
0	3/2		−173.631 32	−172.703 90	−171.406 03
1	3/2		−113.700 85	−112.830 97	−111.614 45
0	3/2		−93.907 32	−92.941 97	−91.590 69
2	3/2		−64.324 54	−63.566 57	−62.506 65
0	5/2			−74.508 93	−73.191 79
1	5/2			−25.829 78	−24.615 72

Derived Spectroscopic Parameters

n	$\|P\|$	$E-E_0$	B	D
0	1/2	36.960 23	0.1978	9.6×10^{-6}
0	1/2	74.216 47	0.2009	9.3×10^{-6}
0,1	1/2	86.007 57	0.1861	1.5×10^{-5}
0,1	1/2	95.466 53	0.1796	6.6×10^{-6}
0	3/2		0.1855	6.1×10^{-6}
1	3/2	59.947 64	0.1741	1.6×10^{-5}
0	3/2	79.712 65	0.1931	2.6×10^{-6}
2	3/2	109.357 53	0.1517	1.5×10^{-5}
0	5/2	99.930 05	0.1883	9.2×10^{-6}
1	5/2	147.645 78	0.1737	1.9×10^{-5}

Excitation of the bending vibration to $v_b=1$, with vibrational angular momentum $k=\pm1$, might be expected to produce two states with $|P|=1/2$ and 5/2. These are indeed found. However, the $|\omega|=1/2$ surface is also nearby, and can support additional states of similar energy.

To assist with understanding the energy levels, we have calculated wave functions for the states found in the helicity decoupling calculations. In addition, we have extracted rotational constants by fitting a standard energy formula to the energy levels as a function of J,

$$E(J)=E(0)+B(J(J+1)-P^2)-D(J(J+1)-P^2)^2. \tag{6}$$

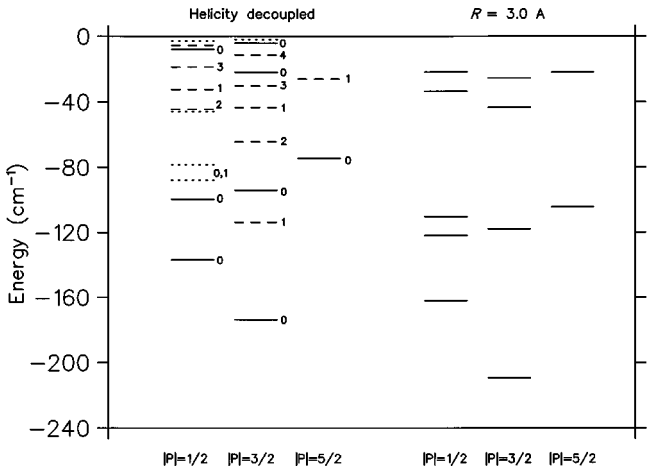

FIG. 3. Pattern of all levels in the helicity decoupled approximation (left), compared to the bending levels calculated by diagonalizing the helicity decoupling matrix at $R=3.0$ Å (right). In the left-hand diagram, solid lines correspond to pure bending states, long dashed lines to stretching excited states, and short dashed lines to states which cannot be unambiguously classified. The assignments have been established on the basis of wave function plots and the labels indicate the number of stretching quanta n.

Selected wave functions are shown in Figs. 4 and 5. Each wave function is shown as a separate contour plot for the components corresponding to atomic spin–orbital functions with $(j_a,|\omega|)=(3/2,3/2)$, $(3/2,1/2)$ and $(1/2,1/2)$.

Even for the lowest vibronic states, there is extensive mixing of $|\omega|=3/2$ and 1/2 character. For $|P|=3/2$, the ground state (at $-174\,cm^{-1}$) has most of its amplitude on the $|\omega|=3/2$ surface, peaked at $\theta=0$, but there is also significant amplitude on the $|\omega|=1/2$ surface, peaked around $\theta=45°$. There is an easily recognizable excited state with stretching quantum number $n=2$ at $-64\,cm^{-1}$ (not shown in the figure). However, the $n=1$ stretching character is split between two states at -114 and $-94\,cm^{-1}$. The lower of these is predominantly the $n=1$ stretch, while the upper contains considerably more population on the $\omega=1/2$ surface, with its density maximum around $\theta=115°$.

The wave functions for the lowest $|P|=1/2$ and 5/2 states (at -137 and $-75\,cm^{-1}$, respectively) are fairly similar to one another; these two states can be interpreted as similar to the lowest $|P|=3/2$ state but with one unit of bending vibration (and hence of bending vibrational angular momentum). However, the two states at -88 and $-78\,cm^{-1}$ are more difficult to assign: their wave functions are fairly localized on the $|\omega|=3/2$ surface, but span the entire angular range on the $|\omega|=1/2$ surface.

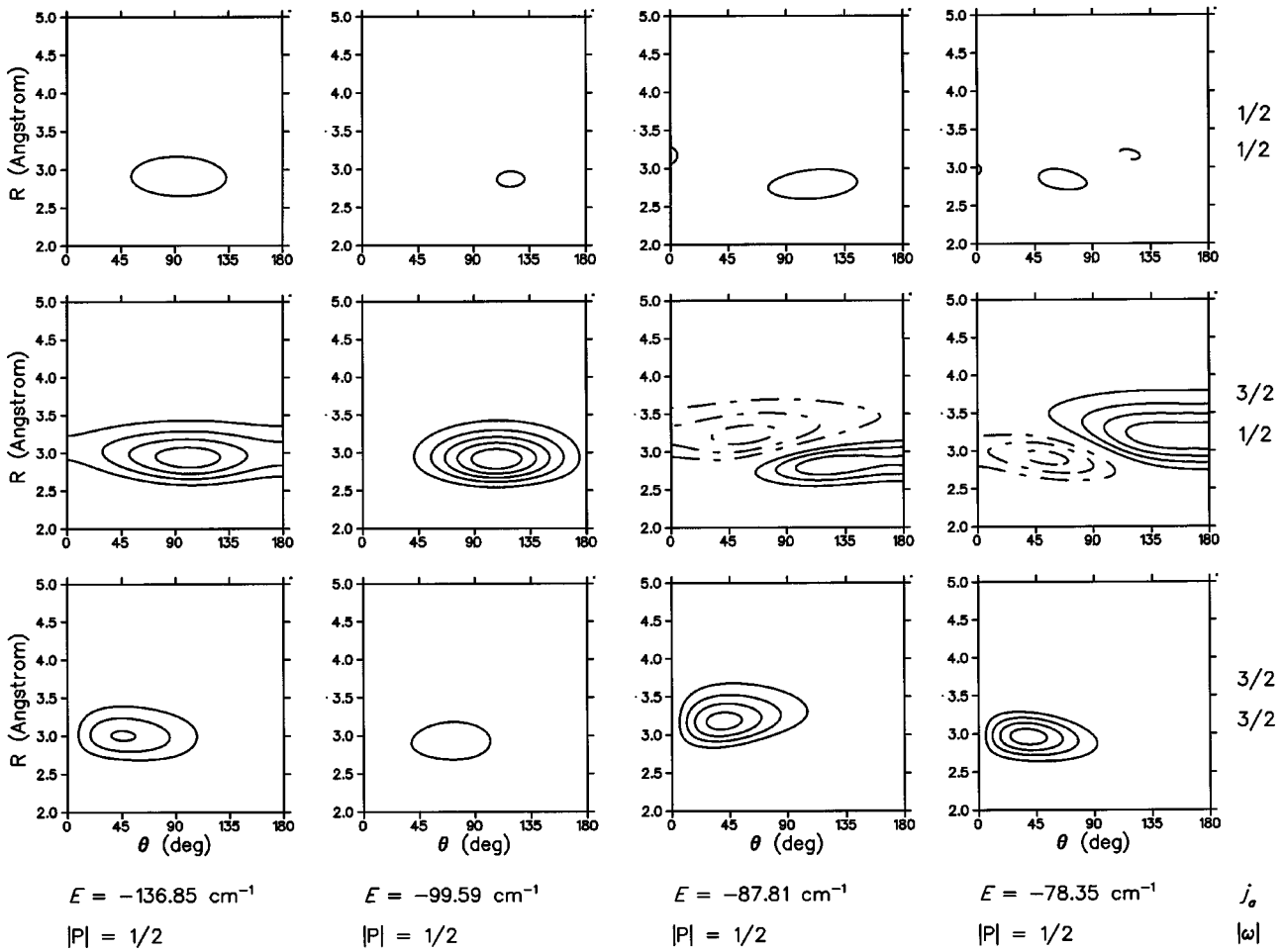

FIG. 4. Wave functions for the lowest four $|P|=1/2$ states of F–HF. Solid and broken lines represent positive and negative lobes of the wave function. For each function, the three panels show the wave function contribution for the $(j_a,|\omega|)$ atomic state indicated on the right.

B. Close-coupling calculations

Helicity decoupling calculations neglect Coriolis couplings and parity splittings in the energy levels. Such splittings could be measured in either microwave, high-resolution infrared, or ultraviolet spectra, so it is worthwhile to investigate them. To do this, we have carried out close-coupling calculations of the lowest few levels, as described in Ref. 10. The close-coupling calculations were performed in the space-fixed representation and produced the energy levels shown in Table II.

The parity splittings behave differently for $|P|=1/2$ and $|P|=3/2$. For $|P|=1/2$ the splitting varies as $2p(J+1/2)$ and for $|P|=3/2$ as $2q(J-1/2)(J+1/2)(J+3/2)$.[9] Table II shows the parity doubling parameters. The e/f parity alternates as a function of J. This effect is similar to λ doubling in diatomic molecules. The splitting decreases with increasing $|P|$ and increases with increasing J.

For some vibrational states, the parity doubling constants are comparable to the rotational constants. In such cases the parity doubling can have a substantial effect on the level pattern.

The states correlating with F $(^2P_{1/2})$ might be spectroscopically observable, but have finite lifetimes because they lie above the threshold for dissociation to HF+F $(^2P_{3/2})$ and can predissociate. We have investigated the lowest such state by performing close-coupling scattering calculations to characterize the scattering resonance. The scattering calculations were performed with the MOLSCAT package[27] and calculated eigenphase sums were fitted to a Breit–Wigner form using the RESFIT program,[28] as described in Ref. 29.

Interestingly, the e and f components have quite different widths. The f component of the lowest $J=1/2$ state for $j_a=1/2$ lies 394.05 cm^{-1} above the $^2P_{3/2}$ threshold (and thus 567.68 cm^{-1} above the ground state). It is bound by 9.90 cm^{-1} with respect to the $^2P_{1/2}$ asymptote. It has a full width at half maximum $\Gamma=0.044\,\mathrm{cm}^{-1}$, corresponding to a lifetime of about 120 ps. Analysis of the partial widths shows that about 55% of the predissociation products are created in the highest energetically accessible state, F $(^2P_{3/2})$+HF $(j=3)$. The corresponding e state lies 0.19 cm^{-1} above the f state, with width $\Gamma=0.0091\,\mathrm{cm}^{-1}$ (corresponding to a lifetime of 583 ps). In this case, about 60% of the predissociation products are created in F $(^2P_{3/2})$+HF $(j=3)$.

We have also performed similar calculations for Cl–HCl, using the potential energy surfaces of Dubernet and Hutson.[10] For this system, the lowest-lying f state correlating with Cl $(^2P_{1/2})$ lies 788.94 cm^{-1} above the $^2P_{3/2}$ asymptote and thus 1062.63 cm^{-1} above the ground state. Its width is

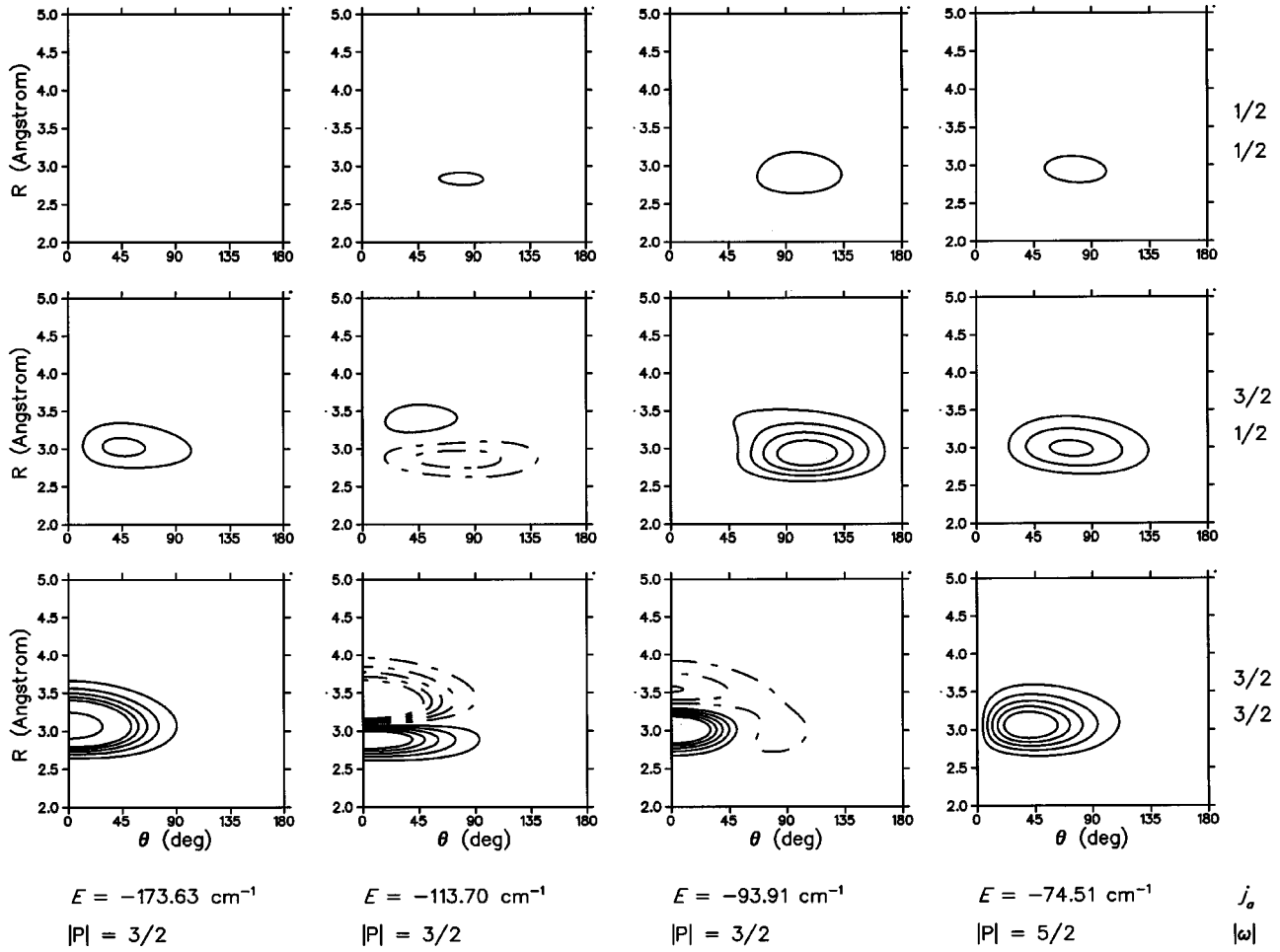

FIG. 5. Wave functions for the lowest three $|P|=3/2$ states and the lowest $|P|=5/2$ state of F–HF. For each function, the three panels show the wave function contribution for the $(j_a,|\omega|)$ atomic state indicated on the right.

$2.26\times10^{-5}\,\mathrm{cm}^{-1}$, corresponding to a lifetime of 235 ns. This time, about 70% of the products are formed in the highest accessible state, Cl $(^2P_{3/2})+\mathrm{HCl}$ $(j=8)$. The e component is $0.10\,\mathrm{cm}^{-1}$ above the $^2P_{3/2}$ asymptote with a width of $1.92\times10^{-5}\,\mathrm{cm}^{-1}$ (corresponding to a lifetime of 277 ns). About 50% of the products are formed in Cl $(^2P_{3/2})$ $+\mathrm{HCl}(j=8)$.

The difference between the lifetimes of F–HF and Cl–HCl is about three orders of magnitude. It arises mostly because of the larger excess energy in the Cl–HCl case, which requires more rotational excitation of the product HX to absorb it.

IV. CONCLUSIONS

The F–HF complex is a fascinating species with a rich spectroscopy. If it can be observed, it will shed light on the mechanism of the F+HF reaction, and especially on the potential energy surfaces in the entrance and exit valleys of the reaction. It is also likely to be one of the products in the ultraviolet photodissociation of HF in HF dimer.

Because the F $(^2P_{3/2})$ atom has a quadrupole moment, the F–HF complex is bound by electrostatic forces in addition to the usual dispersion and induction forces. We have described a model for the three potential energy surfaces that correlate with F $(^2P_{3/2})$ and F $(^2P_{1/2})$, and have used them to carry out bound-state calculations. The lowest surface has a well depth of $317\,\mathrm{cm}^{-1}$, and the ground-state level is bound by $174\,\mathrm{cm}^{-1}$. Intermolecular bending transitions that should have reasonable spectroscopic intensity are predicted around 37 and $99\,\mathrm{cm}^{-1}$. Vibronic wave functions for the lowest few states have been calculated and analyzed, and throw useful light on the energy level pattern.

The best available *ab initio* calculations[15] give well depths somewhat deeper than the present model potentials. It is entirely possible that the present model underestimates the well depths. However, the *ab initio* calculations did not include corrections for basis-set superposition error, so might themselves overestimate the well depths. Either experimental results or more complete *ab initio* calculations are needed to resolve this.

The adiabatic potential well correlating with F $(^2P_{1/2})$ is much shallower than that correlating with F $(^2P_{3/2})$ because the atom has no quadrupole moment in its $^2P_{1/2}$ state. The resulting well is only $52\,\mathrm{cm}^{-1}$ deep in our model. The states supported by this well can predissociate to form F $(^2P_{3/2})$ $+\mathrm{HF}$. However, the lowest such state has calculated widths of $0.044\,\mathrm{cm}^{-1}$ (f) and $0.0091\,\mathrm{cm}^{-1}$ (e), so may still be observable in a high-resolution experiment.

TABLE II. Energy levels and spectroscopic parameters from close-coupling calculations for F–HF. All quantities are given in cm^{-1}, with energy levels relative to the energy of $F(^2P_{3/2})+HF(j=0)$.

n	parity	$\|P\|$	$J=1/2$	$J=3/2$	$J=5/2$
0	e	1/2	−137.135 36	−135.693 44	−136.131 85
0	f	1/2	−136.566 75	−136.830 11	−134.428 23
0	e	1/2	−99.620 83	−98.999 32	−98.225 41
0	f	1/2	−99.571 03	−99.102 86	−98.060 58
0,1	e	1/2	−88.013 01	−86.831 30	−86.917 18
0,1	f	1/2	−87.602 93	−87.652 68	−85.682 11
0,1	e	1/2	−78.593 78	−77.325 13	−77.618 88
0,1	f	1/2	−78.111 12	−78.288 89	−76.177 15
0	f	3/2	⋯	−173.634 03	−172.716 83
0	e	3/2	⋯	−173.634 05	−172.716 76
1	f	3/2	⋯	−113.706 44	−112.850 55
1	e	3/2	⋯	−113.706 59	−112.849 95
0	f	3/2	⋯	−93.873 87	−92.844 82
0	e	3/2	⋯	−93.869 53	−92.861 86
2	f	3/2	⋯	−64.326 78	−63.576 02
2	e	3/2	⋯	−64.326 85	−63.575 75
0	e	5/2	⋯	⋯	−74.509 93
0	f	5/2	⋯	⋯	−74.509 92

Derived Spectroscopic Parameters

n	$\|P\|$	E	B	p	q
0	1/2	−136.949 18	0.1964	0.122	
0	1/2	−99.686 74	0.1816	0.012	
0,1	1/2	−87.902 09	0.1885	0.088	
0,1	1/2	−78.443 34	0.1818	0.103	
0	3/2	−173.909 21	0.1835		6×10^{-6}
1	3/2	−113.693 39	0.1713		5×10^{-6}
0	3/2	−94.185 99	0.2050		-1×10^{-3}
2	3/2	−64.552 09	0.1502		2×10^{-5}

ACKNOWLEDGMENTS

M. M. acknowledges financial support from the Schweizerischer Nationalfonds zur Förderung der wissenschaftlichen Forschung. The calculations were carried out on a Silicon Graphics Origin 2000 computer system, which was purchased with funding from the Engineering and Physical Sciences Research Council. We are grateful to Dr. Lydia Heck for computational assistance.

[1] J. M. Hutson, J. Chem. Phys. **96**, 6752 (1992).
[2] J. M. Hutson, J. Phys. Chem. **96**, 4237 (1992).
[3] R. J. Le Roy, C. Bissonette, T. H. Wu, A. K. Dham, and W. J. Meath, Faraday Discuss. Chem. Soc. **97**, 81 (1994).
[4] M. J. Elrod and R. J. Saykally, J. Chem. Phys. **103**, 933 (1995).
[5] J. M. Hutson, A. Ernesti, M. M. Law, C. F. Roche, and R. J. Wheatley, J. Chem. Phys. **105**, 9130 (1996).
[6] M. Quack and M. Suhm, J. Chem. Phys. **95**, 28 (1991).
[7] M. H. Alexander, Chem. Phys. **92**, 337 (1985).
[8] M.-L. Dubernet, D. R. Flower, and J. M. Hutson, J. Chem. Phys. **94**, 7602 (1991).
[9] W. H. Green and M. I. Lester, J. Chem. Phys. **96**, 2573 (1992).
[10] M.-L. Dubernet and J. M. Hutson, J. Phys. Chem. **98**, 5844 (1994).
[11] C. S. Maierle, G. C. Schatz, M. S. Gordon, P. McCabe, and J. N. L. Connor, J. Chem. Soc., Faraday Trans. **93**, 709 (1997).
[12] A. J. Dobbyn, J. N. L. Connor, N. A. Besley, P. J. Knowles, and G. C. Schatz, Phys. Chem. Chem. Phys. **1**, 957 (1999).
[13] K. Liu, A. Kolessov, J. W. Partin, I. Bezel, and C. Wittig, Chem. Phys. Lett. **299**, 374 (1999).
[14] R. Preuss, S. D. Peyerimhoff, and R. J. Buenker, J. Mol. Struct. **40**, 117 (1977).
[15] M. Bittererová and S. Biscupič, Chem. Phys. Lett. **299**, 145 (1999). Note that in Table V the second column should be headed $R_{HF'}$, and that all the energies should be negative.
[16] R. D. Hunt and L. Andrews, J. Chem. Phys. **87**, 6819 (1987).
[17] K. Kawaguchi and E. Hirota, J. Mol. Struct. **352**, 389 (1995).
[18] P. Cipollini, M. E. Crestoni, and S. Fornarini, J. Am. Chem. Soc. **119**, 9499 (1997).
[19] M.-L. Dubernet and J. M. Hutson, J. Chem. Phys. **101**, 1939 (1994).
[20] M. Meuwly and J. M. Hutson, J. Chem. Phys. **110**, 8338 (1999).
[21] T. Y. Chang, Rev. Mod. Phys. **39**, 911 (1967).
[22] V. Aquilanti, R. Candori, D. Cappelletti, E. Luzzatti, and F. Pirani, Chem. Phys. **145**, 293 (1990).
[23] R. A. Aziz and M. J. Slaman, Chem. Phys. **130**, 187 (1989).
[24] BOUND computer program, Version 5, J. M. Hutson, distributed by Collaborative Computational Project No. 6 of the UK Engineering and Physical Sciences Research Council, 1993.
[25] B. R. Johnson, J. Comput. Phys. **13**, 445 (1973).
[26] J. M. Hutson, Comput. Phys. Commun. **84**, 1 (1994).
[27] MOLSCAT computer program, Version 14, J. M. Hutson and S. Green, distributed by Collaborative Computational Project No. 6 of the UK Engineering and Physical Sciences Research Council, 1994.
[28] RESFIT computer program, J. M. Hutson and C. J. Ashton, 1982, available from the author.
[29] C. J. Ashton, M. S. Child, and J. M. Hutson, J. Chem. Phys. **78**, 4025 (1983).